Pressure/temperature/substitution-induced melting of *A*-site charge disproportionation in $Bi_{1-x}La_xNiO_3$ ($0 \leqslant x \leqslant 0.5$)

S. Ishiwata,[1,*] M. Azuma,[1,2] M. Hanawa,[2,3] Y. Moritomo,[2,3] Y. Ohishi,[4] K. Kato,[4,5] M. Takata,[4,5] E. Nishibori,[3] M. Sakata,[3] I. Terasaki,[6] and M. Takano[1]

[1]*Institute for Chemical Research, Kyoto University, Gokashou, Uji 611-0011, Japan*

[2]*PRESTO, Japan Science and Technology Agency (JST), Kawaguchi, Saitama 332-0012, Japan*

[3]*Department of Applied Physics, Nagoya University, Furo-cho, Chigusa-ku, Nagoya 464-8601, Japan*

[4]*JASRI, Japan Synchrotron Radiation Research Institute, 1-1-1 Kouto, Mikazuki-cho, Sayo-gun, Hyogo 679-5198, Japan*

[5]*CREST, Japan Science and Technology Agency (JST), Kawaguchi, Saitama 332-0012, Japan*

[6]*Department of Applied Physics, Waseda University, Ookubo, Shinjuku, Tokyo 169-8555, Japan*

(Received 2 February 2005; revised manuscript received 13 May 2005; published 5 July 2005)

Metal-insulator transitions strongly coupled with lattice were found in $Bi_{1-x}La_xNiO_3$. Synchrotron x-ray powder diffraction revealed that pressure ($P \sim 3$ GPa, $T=300$ K), temperature ($T \sim 340$ K, $x=0.05$), and La substitution ($x \sim 0.075$, $T=300$ K) caused the similar structural change from a triclinic (insulating) to an orthorhombic (metallic) symmetry, suggesting melting of the *A*-site charge disproportionation. Comparing crystal structure and physical properties with the other $ANiO_3$ series, an electronic state of the metallic phase can be described as $[A^{3+}\underline{L}^{\delta}, Ni^{2+}\underline{L}^{1-\delta}]$, where a ligand-hole $\underline{L}$ contributes to a conductivity. We depicted a schematic *P-T* phase diagram of $BiNiO_3$ including a critical point (3 GPa, 300 K) and an inhomogeneous region, which implies universality of ligand-hole dynamics in $ANiO_3$ (*A*=Bi, Pr, Nd…).

DOI: 10.1103/PhysRevB.72.045104 PACS number(s): 71.30.+h, 61.10.Nz, 74.62.Dh, 75.40.Cx

I. INTRODUCTION

Charge ordering is a common phenomenon in mixed-valence transition-metal oxides, but it attracts much attention because of competition with fascinating metallic behavior exhibiting superconductivity or giant magnetoresistance.[1–4] The competition between them has been keenly discussed as a clue for understanding the origin of such striking properties.[2,3] In addition to the mixed-valence systems, several integer-valence perovskite oxides such as $CaFeO_3$ and $ANiO_3$ (*A*=Y, Pr, Nd…) also show a charge-ordering transition described as $2M^{n+} \rightarrow M^{(n-\delta)+} + M^{(n+\delta)+}$, which is called charge disproportionation (CD).[5–9] CD can be detected as a symmetry breaking from orthorhombic ($GdFeO_3$-type structure) to monoclinic symmetry, which is caused by the breathing-type cooperative displacements like O--M^{n+}--O --M^{n+}--O$\rightarrow$O---$M^{(n-\delta)+}$---O-$M^{(n+\delta)+}$-O.

The metal-insulator (MI) transition in perovskite $ANiO_3$ series, associated with CD, has been studied systematically by substitution of *A* site and/or application of pressure.[10–14] The MI transition temperature, T_{MI}, decreases monotonically as the size of an *A*-site ion or external pressure increases, i.e., the conduction band made of 3*d*(Ni) and 2*p*(O) orbitals becomes wider as the mean Ni-O-Ni bond angle increases. We should note here that the electronic properties of oxides containing an unusually high-valent ion such as Fe^{4+} and Ni^{3+} may be dominated by an oxygen-hole character which stems from strong *p-d* hybridization.[15–17] Photoemission spectroscopic studies suggest that the realistic electronic state of Ni^{3+} in $(NiO_6)^{9-}$ octahedron is close to $Ni^{2+}\underline{L}$ ($\underline{L}$: a ligand hole; a hole in a ligand oxygen 2*p* orbital).[16] CD in AMO_3 could thus be expressed as $2M^{n+}\underline{L} \rightarrow M^{n+} + M^{n+}\underline{L}^{2\delta}$, where ligand holes play a crucial role.

Recently, we have found a unique fashion of CD in a triclinic (space group; $P\bar{1}$) perovskite $BiNiO_3$. The crystal structure analysis indicates that the valence state is not $Bi^{3+}Ni^{3+}O_3$ or $Bi^{3+}Ni^{(3-\delta)+}{}_{0.5}Ni^{(3+\delta)+}{}_{0.5}O_3$, but $Bi^{3+}{}_{0.5}Bi^{5+}{}_{0.5}Ni^{2+}O_3$ (Ref. 18). The divalent nature of Ni ions and the triclinically distorted structure, caused by the *A*-site CD, lead to insulating behavior. Since "Bi^{5+}" has a very deep open 6*s* level, and such a high valence state at the *A* site is not stable from the viewpoint of Madelung potential energy,[19] the realistic charge configuration of Bi^{5+} should be expressed as $Bi^{3+}\underline{L}^2$. That is, ligand holes are trapped and ordered in the Bi-O sublattice rather than in the Ni-O sublattice. Bi^{4+} is a common ion showing CD as reported in $BaBiO_3$, where an antibonding 6*s*(Bi)-2*p*(O) conduction band produces superconductivity by an appropriate substitution.[20,21] In the case of $BiNiO_3$, a competition between $Bi^{3+}\underline{L}$ (Bi^{4+}) and $Ni^{2+}\underline{L}$ (Ni^{3+}) is expected to exhibit unprecedented localization-delocalization transitions of ligand holes. Indeed, we have observed a structural transition of $BiNiO_3$ to an orthorhombic symmetry at 513 K (Refs. 18,22). However, the physical properties of the orthorhombic phase is unclear because of a partial decomposition due to a thermal oxygen loss.

In this paper, we report structural and physical properties of $Bi_{1-x}La_xNiO_3$ as functions of pressure ($x=0$), temperature ($x=0.05$), and La content ($0 \leqslant x \leqslant 0.5$). These data consistently demonstrate melting of *A*-site CD, accompanied with insulator (triclinic) to metal (orthorhombic) transitions dominated by ligand-hole dynamics.

II. EXPERIMENT

Polycrystalline samples of $Bi_{1-x}La_xNiO_3$ ($x=0$, 0.05, 0.075, 0.1, 0.2, 0.5) were obtained by high-pressure syntheses as described before.[18] A precursor was

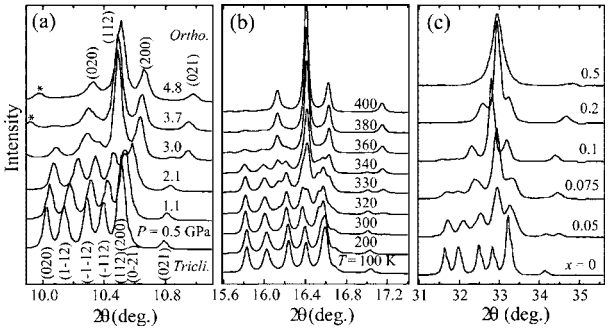

FIG. 1. XRD patterns of $BiNiO_3$ at (a) 0.5, 1.1, 2.1, 3.0, 3.7, and 4.8 GPa with $\lambda=0.4966$ Å, (b) $Bi_{0.95}La_{0.05}NiO_3$ at 100, 200, 300, 320, 330, 340, 360, 380, and 400 K with $\lambda=0.776$ Å, and (c) $Bi_{1-x}La_xNiO_3$ ($x=0$, 0.05, 0.075, 0.1, 0.2, and 0.5) with Cu $K\alpha$ at room temperature, traversing the phase transition between triclinic (with CD) and orthorhombic (without CD) perovskite. An impurity phase was indicated by an asterisk.

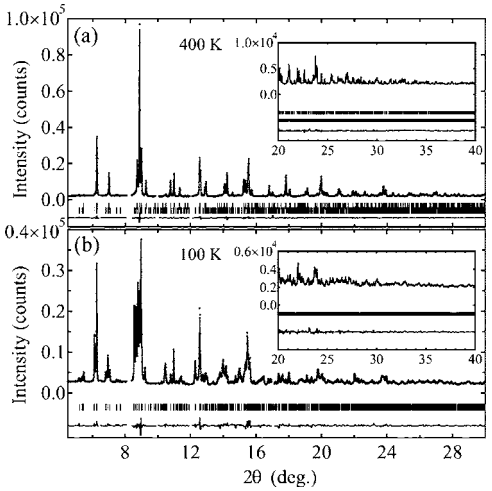

FIG. 2. Measured (+), calculated (line), and differential (bottom line) SXRD patterns for $Bi_{0.95}La_{0.05}NiO_3$ at (a) 400 K and (b) 100 K. The ticks indicate the positions of the reflections: upper in (a), orthorhombic; lower in (a) and (b), triclinic. The mass fraction of a triclinic phase at 400 K is 6%.

prepared by dissolving stoichiometric amounts of Bi_2O_3, La_2O_3, and Ni in nitric acid, followed by heating at 730 °C in air for 6 h. A mixture of the precursor and an oxidizer $KClO_4$ (20 wt. % to the precursor) was treated at 1000 °C and 6 GPa for 30 min. The obtained samples were washed in distilled water to dissolve KCl. The samples used for measurements of resistivity were pressed to be dense at 6 GPa at room temperature.

Powder x-ray diffraction (XRD) data for phase identification were recorded on a Rigaku RINT 2500 diffractometer using Cu $K\alpha$ radiation. Surface XRD (SXRD) data of $BiNiO_3$ under high pressure and these of $Bi_{1-x}La_xNiO_3$ at ambient pressure (AP) were collected using a diamond-anvil cell (DAC) at beam line BL10XU and a large Debye-Scherrer camera at BL02B2 (Ref. 23) of SPring-8, respectively. The granularity of the powder samples were homogenized to 2–3 μm in diameter by the precipitation method. For DAC experiments ethanol/methanol mixture was used as a pressure-transmitting medium. To reduce the absorption effect of Bi ions, we selected as short wavelength as $\lambda=0.4966$ Å for DAC experiments and $\lambda=0.420\,84$ Å for structure analyses of La-substituted samples. The diffraction data for $Bi_{0.95}La_{0.05}NiO_3$ were taken between 100 and 400 K with N_2 gas flow apparatus at 0.776 Å. All the data were analyzed by the Rietveld method using a RIETAN 2000 program.[24]

Pressure dependence of dc resistivity was measured by a two-probe method using a cubic-anvil-type high-pressure apparatus. Electrical resistivities between 2 and 400 K were measured by a four-probe method using a Quantum Design PPMS at a rate of 2 K/min. Thermopower was measured by a steady-state technique with a typical temperature gradient of 1 K/mm, and the contribution of the voltage leads was carefully subtracted. dc magnetic susceptibility measurements were performed with a Quantum Design MPMS XL SQUID magnetometer in an external magnetic field of 0.1 T on cooling.

III. RESULTS

First of all, we survey several XRD patterns indicating structural phase transitions caused by pressure, temperature, and La substitution [Figs. 1(a)–1(c)]. In Fig. 1(a), five main peaks in the diffraction pattern at the bottom, characteristic of the triclinic cell, decreased to three of the orthorhombic cell; a structural transition from the AP phase to the high-pressure (HP) phase. The XRD pattern of the HP phase at 3 GPa was indexed assuming an orthorhombic unit cell of $5.32\times5.50\times7.62$ Å ($GdFeO_3$-type cell). The similar behavior can be seen in the SXRD patterns for $Bi_{0.95}La_{0.05}NiO_3$ taken at various temperatures [Fig. 1(b)]. The low-temperature (LT) and high-temperature (HT) phases were indexed with triclinic ($P\bar{1}$) and orthorhombic ($Pbnm$) symmetries, respectively (see Fig. 2). The $GdFeO_3$-type orthorhombic structure ensures melting of CD in the HP and HT phases, for there is only one equivalent Bi site. Figure 1(c) shows the XRD patterns of $Bi_{1-x}La_xNiO_3$ taken at room temperature. With increasing La content, x, the number of the main peaks changes gradually from five to three via the composition with $x=0.075$, where these two phases coexist.

Figures 3(a)–3(d) show evolutions of structural parameters under high pressure with traversing phase transition from triclinic (insulating) to orthorhombic (metallic) symmetry. The unit-cell volume V and the lattice parameters a, b, and c decrease steeply across the transition to the HP phase (volume change at 3 GPa is 2.5%). Since the unit-cell volume of the perovskite-type structure is dominated by the B-O bond distance, the mean Ni-O distance of the HP phase is expected to be shorter than that of the AP phase. On increasing pressure, triclinic angles α, β, and γ tend to merge into 90°, but still are not unified at 3 GPa. In accordance with the structural phase transition, pressure-dependent resistivity of $BiNiO_3$ at room temperature ($T=300$ K) shows a steep drop by several orders of magnitude around 3 GPa, suggesting that an external pressure causes delocalization of ligand holes trapped in the Bi-O sublattice [Fig. 3(d)].[25]

The temperature-dependent variations of unit-cell volume, lattice parameters, unit-cell angles, and resistivity of $Bi_{0.95}La_{0.05}NiO_3$ are quite similar to those as function of

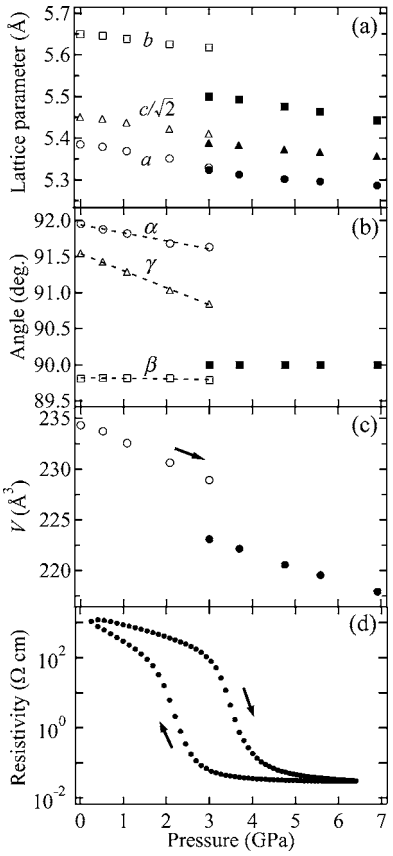

FIG. 3. Pressure dependence of (a) lattice parameters, (b) unit-cell angles, (c) unit-cell volume (Z=4), and (d) resistivity of $BiNiO_3$ at room temperature (T=300 K). In (a)–(c), the data were collected with increasing pressure. The open and closed symbols signify the AP and HP phases, respectively. The dashed lines in (b) are guides to the eyes.

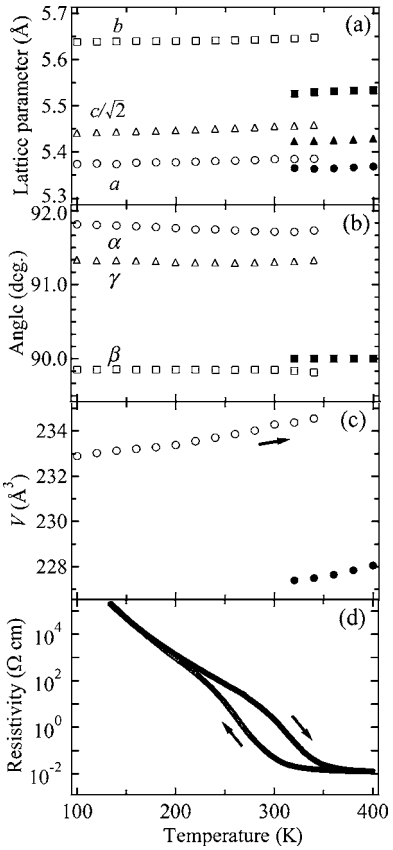

FIG. 4. Temperature dependence of (a) lattice parameters, (b) unit-cell angles, (c) unit-cell volume (Z=4), and resistivity of $Bi_{0.95}La_{0.05}NiO_3$. In (a)–(c), the data were collected on heating. The open and filled symbols signify the LT and HT phases, respectively.

pressure [Figs. 4(a)–4(d)]. The discontinuity and coexisting of two phases on the verge of 340 K indicate the first-order nature of this transition. The magnitude of the volume contraction at 340 K ($\Delta V/V=-3\%$) is comparable to that between the AP and HP phases of $BiNiO_3$. Focused on the structural and the transport behavior, both increasing temperature and pressure induce melting of CD and delocalization of carriers in the same manner.

By controlling La content, x, in $Bi_{1-x}La_xNiO_3$, similar plots of structural parameters and resistivity can be seen at 300 K [Figs. 5(a)–5(d)]. On increasing x, the resistivity decreases by 5–6 orders of magnitude with the decrease of unit-cell volume, $\Delta V/V=-3\%$, as reported previously [Fig. 4(d)].[26] La substitution for x=0.075 leads to symmetrical change from the triclinic to the orthorhombic phase, which is metallic without CD, corresponding roughly to the applied pressure of 3 GPa. However, the SXRD data indicates the presence of a small amount of the triclinic phase for x=0.1 (16.7% wt. fraction), whereas no triclinic phase can be detected for x=0.2.

As can be seen in Fig. 6(a), the La-substituted samples show metallic behavior, and diffuse MI transitions with large thermal hystereses are observed for $x \leqslant 0.1$. The samples with x=0.075 and 0.1 show the reentrant metallic behavior at low temperatures, suggesting incompleteness of the MI transition. The thermopower, S, for x=0.075 and 0.1 are roughly proportional to T at low temperatures as observed in the metallic compound $LaNiO_3$ [Fig. 6(b)].[27] This behavior is in contrast with that for x=0.05, which diverges below T_{MI}, as a hallmark of an insulator. We will discuss this point later.

Figures 6(c) and 6(d) show the temperature dependence of susceptibility and inverse susceptibility of $Bi_{1-x}La_xNiO_3$, measured in a magnetic field of 0.1 T on cooling. Surprisingly, all the compositions undergo antiferromagnetic ordering near 300 K, and the Neel ordering temperature, T_N, seems to have no correlation with x, which is a remarkable dissimilarity to the other members of $ANiO_3$. Below T_N, ferromagnetic moment due to canted spins emerges. In addition, the paramagnetic susceptibility for all samples seemingly obeys the Curie-Weiss law as shown in Fig. 6(d).

So far, we have demonstrated that increasing pressure, temperature, and La substitution lead to the orthorhombic phase where A-site CD is absent. Here, we take a look at the detailed structural features to compare them quantitatively with each other. Figure 7(a) summarizes $GdFeO_3$-type distortion of $ANiO_3$, represented by b/a where a and b denote lattice parameters ($BiNiO_3$ has also $GdFeO_3$-type unit cell with triclinic distortion). The value b/a decreases linearly as the A-site ion becomes larger from Y to Pr (taken from Ref. 10), i.e., as the tolerance factor, t $[=(r_A+r_O)/\sqrt{2}(r_{Ni}+r_O)]$,

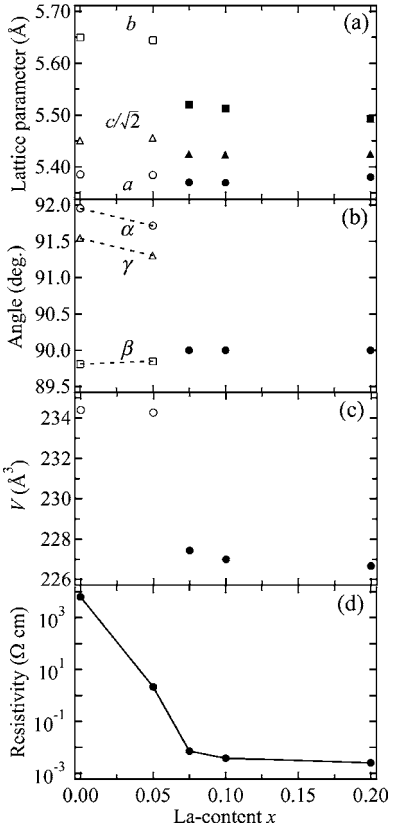

FIG. 5. La-content, x, dependence of (a) lattice parameters, (b) unit-cell angles, (c) unit-cell volume (Z=4), and resistivity of $Bi_{1-x}La_xNiO_3$ at room temperature (T=300 K). The dashed lines in (b) are guides to the eyes.

becomes larger. Suppose the valence state of the A-site ion is trivalent, a linear relationship is expected between b/a and r_A as plotted in Fig. 7(a). However, $Bi_{1-x}La_xNiO_3$ (x =0.1, 0.2) and $BiNiO_3$ show the remarkable upward deviation from the expected line (even larger than $SmNiO_3$), which indicates that the effective tolerance factors are smaller than the expected values assuming the trivalent ionic radii for each cations. This deviation is derived from the misestimation of its charge distribution; i.e., the realistic electronic state for $Bi_{1-x}La_xNiO_3$ should be denoted as [$A^{3+}\underline{L}^{\delta}$, $Ni^{2+}\underline{L}^{1-\delta}$] ($A$=$Bi_{1-x}La_x$). δ is equal to 1 for x=0 ($BiNiO_3$). δ decreases with increasing x, and eventually δ is supposed to be zero when x becomes 1 ($LaNiO_3$). The remaining ligand holes in the A site are actually confirmed by the mean Ni-O bond distances of $Bi_{1-x}La_xNiO_3$, 1.973 Å (x =0.2) ~ 2.091 Å (x=0) (see Table I), which are significantly longer than the predicted value for Ni^{3+}-O^{2-} (1.937 Å). By using the variation of the indicator, b/a, we tried to make quantitative comparison between La content, x, and pressure, P [Fig. 7(b)]. The plots clearly show equivalency of these parameters, allowing us to interchange La content with chemical pressure.[28]

IV. DISCUSSIONS

Our scenario deduced from structure analysis, resistivity, and susceptibility measurements is as follows. The AP phase

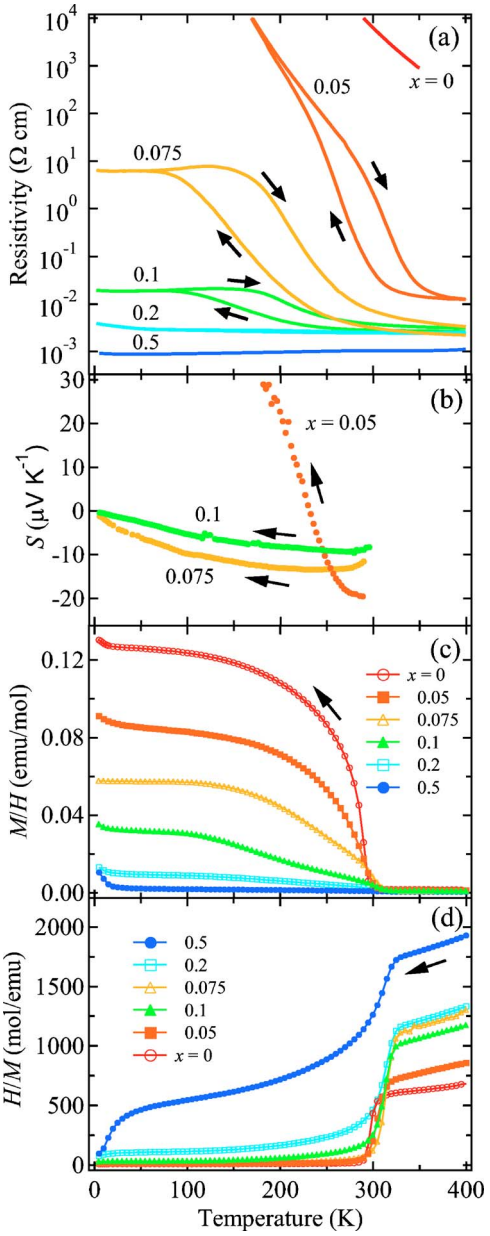

FIG. 6. (Color online) Temperature dependence of (a) resistivity, (b) Seebeck coefficient, (c) magnetic susceptibility, and (d) inverse magnetic susceptibility of $Bi_{1-x}La_xNiO_3$.

of $BiNiO_3$ and the LT phase of $Bi_{0.95}La_{0.05}NiO_3$ have the same structure and electronic state, described as [$A^{3+}{}_{0.5}$ +$A^{3+}\underline{L}^{2}{}_{0.5}$, Ni^{2+}] (A=Bi or $Bi_{0.95}La_{0.05}$); an antiferromagnetic insulator due to the divalent nature of Ni ion. Increasing pressure, La content, or temperature suppresses the development of CD as confirmed by symmetry change to orthorhombic perovskite, giving rise to conductive behavior. The steep drop of the resistivity under high pressure has clearly indicated that $BiNiO_3$ is rather conductive when CD is absent. Although we failed to determine the atomic fractional coordinates for the HP phase, a lattice contraction accompanied by the symmetry change across the phase transition suggests that the electronic configuration of the HP phase is almost the same as the orthorhombic phase of $Bi_{1-x}La_xNiO_3$. As

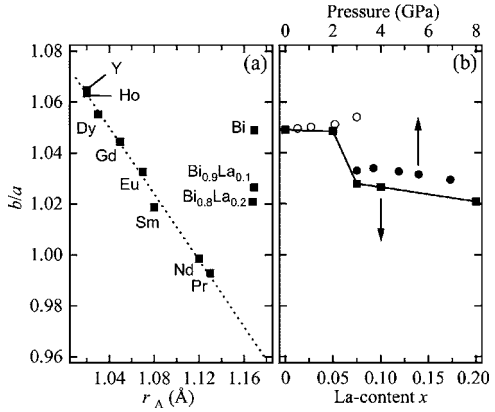

FIG. 7. Magnitude of the orthorhombic distortion, b/a, of $ANiO_3$ as a function of the mean ionic radii of A-site ion r_A (a), and that of $Bi_{1-x}La_xNiO_3$ as a function of La content x and pressure (b). The ionic radii for trivalent ions with eight coordination were adopted for r_A.

proposed in Fig. 7(a), we describe the electronic state of the orthorhombic phase as $[A^{3+}\underline{L}^{\delta}, Ni^{2+}\underline{L}^{1-\delta}]$ $(A=Bi_{1-x}La_x)$.

Next, let us compare structural and physical properties of the orthorhombic phase of $Bi_{1-x}La_xNiO_3$ with those of $SmNiO_3$ ($T_{MI}=400$ K, $T_N=225$ K). Structural analyses based on SXRD were performed for the samples with $x=0$ (given in Ref. 18), 0.05 (see Fig. 2), 0.1, and 0.2; the refined structure parameters being listed in Table I. In comparison with $SmNiO_3$, the mean Ni-O-Ni angles of $Bi_{1-x}La_xNiO_3$ ($151.4°-153.4°$, $0.05\leqslant x\leqslant 0.2$) are comparable or even smaller ($SmNiO_3$; 153.2°), and the mean Ni-O bond distance (1.973–1.986 Å) is longer ($SmNiO_3$; 1.952 Å) (Ref. 29), which suggests that the conduction band made of $3d$ and $2p$ orbitals is smaller than that of $SmNiO_3$. Never theless, $Bi_{0.8}La_{0.2}NiO_3$ keeps metallic-like behavior far below T_{MI} of $SmNiO_3$. This is ascribable to a strong hybridization between $6s$(Bi) and $2p$(O), being consistent with the presumed electronic configuration $[A^{3+}\underline{L}^{\delta}, Ni^{2+}\underline{L}^{1-\delta}]$ $(A=Bi_{1-x}La_x)$. Consequently, the insulator to metal transition in $Bi_{1-x}La_xNiO_3$ should be expressed as $[A^{3+}{}_{0.5}+A^{3+}\underline{L}^{2}{}_{0.5}, Ni^{2+}]\rightarrow[A^{3+}\underline{L}^{\delta}, Ni^{2+}\underline{L}^{1-\delta}]$. As suggested by the Ni-O bond length, a considerable amount of ligand holes exist around the A site even in the orthorhombic phase, which bears localized spins of Ni^{2+} ($S=1$). This appears to be consistent with the composition-independent T_N of $Bi_{1-x}La_xNiO_3$. Of course, the possibility of the mixing of magnetic (insulating) triclinic phase in the metallic orthorhombic phase as the reason for the composition-independent T_N cannot be ruled out at this stage. Such mixings were indeed detected by the XRD studies for $x\leqslant 1$ samples at 300 K. Relatively high T_N (~300 K) of $Bi_{1-x}La_xNiO_3$, compared with the other $ANiO_3$ series ($T_N=225$ K for $SmNiO_3$ is the highest), could be attributed to the divalent nature of Ni ions and/or the additional superexchange interaction via Ni-O-A-O-Ni in which the role of ligand hole is demonstrated explicitly.

The reentrant metallic behavior without anomaly in the thermopower implies that nanoscale islands of the insulating LT phase grows in the matrix of the metallic HT phase at low temperatures. Note that the insulating islands do not contribute to the thermopower. On decreasing temperature, growth of the islands freezes for the sake of gain of the elastic strain energy, accompanied by a large volume change, just like in relaxor ferroelectrics.[30] We call this coexisting state (insulating icebergs on the metallic sea) 'ligand-hole inhomogeneity'. These insulating icebergs are too small to be detected by x-ray diffraction. In the composition with $x=0.05$, the islands grow into the continent surrounding the metallic sea, making the system insulator and the triclinic perovskite. The large thermal hysteresis in resistivity could be attributed not

TABLE I. Structural parameters together with reliability factors for $Bi_{1-x}La_xNiO_3$.

	(i)[a]	(ii)	(iii)	(iv)	(v)
Parameters (unit)	$x=0$	$x=0.05$	$x=0.05$	$x=0.1$	$x=0.2$
T (K)	300	100	400	300	300
a (Å)	5.3852(2)	5.3732(2)	5.367 23(6)	5.369 61(7)	5.380 25(10)
b (Å)	5.6498(2)	5.6372(2)	5.532 00(6)	5.512 55(7)	5.492 85(9)
c (Å)	7.7078(3)	7.6941(3)	7.674 12(9)	7.668 68(11)	7.670 17(16)
a (deg)	91.9529(10)	91.792(2)			
b (deg)	89.8097(9)	89.853(2)			
g (deg)	91.5411(9)	91.307(2)			
V (Å^3)	234.29(1)	232.88(1)	227.437(5)	226.995(5)	226.676(8)
$\langle A^{3+}\text{-O}\rangle_8$ (Å)	2.564	2.541	2.492	2.495	2.500
$\langle A^{5+}\text{-O}\rangle_6$ (Å)	2.135	2.165			
$\langle\text{Ni-O}\rangle_6$ (Å)	2.091	2.078	1.986	1.980	1.973
$\langle\text{Ni-O-Ni}\rangle$ (deg)	137	138	151.4	152.2	153.4
R_{wp} (%)	2.72	3.89	3.39	3.71	3.90
R_I (%)	1.35	0.91	1.90	0.82	1.19
Space group	$P\bar{1}$	$P\bar{1}$	*Pbnm*	*Pbnm*	*Pbnm*

[a]From Ref. 18.

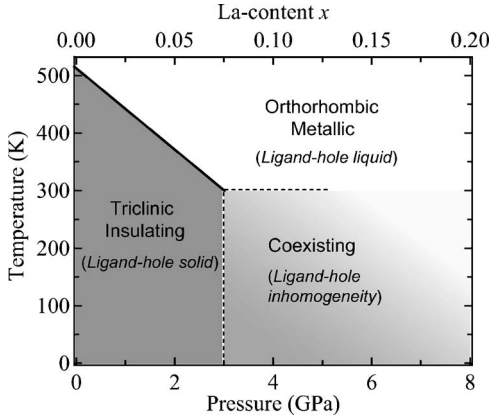

FIG. 8. Schematic phase diagram of $Bi_{1-x}La_xNiO_3$ as functions of pressure, La content x, and temperature.

only to the first-order character of the phase transition but also to the local fluctuation induced by a martensiticlike character of transformation between the LT and HT phases. The similar hysteretic behavior has also been reported for $PrNiO_3$ and $NdNiO_3$ (Refs. 11,12,31).

The aforementioned results are summarized in a schematic phase diagram shown in Fig. 8. The phase boundary between the triclinic (insulating) and the orthorhombic (metallic) phases was extrapolated from the structural transitions of $BiNiO_3$ at $(P,T)=(0,513)$ and (3,300), leading to a rate $\partial T_{\mathrm{MI}}/\partial P=-71$ K. In the case for $ANiO_3$ (A=Pr, Nd), the rate $\partial T_{\mathrm{MI}}/\partial P=-42$ K and $\partial T_{\mathrm{MI}}/\partial P=-76$ K have reported by Obradors *et al.* and Canfield *et al.*, respectively.[11,12] Given that melting of CD in all series of $ANiO_3$ (A=Bi, Pr, Nd, …) is a phase transition from a solid to a liquid state of ligand holes in $2p$ orbitals, the pressure effect on T_{MI} can be qualitatively explained with the Clausius-Clapeyron equation written as $(\partial P/\partial T_{\mathrm{MI}})_{\Delta G}=\Delta S/\Delta V$. On the phase transition from a solid to a liquid state of the ligand holes, $\Delta S>0$ (an entropy change from an ordered state to a disordered state is positive) and $\Delta V/V=-2.5\%$ for $BiNiO_3$ and -0.25% for $PrNiO_3$ (Ref. 32) are given, leading to the inequality $(\partial T_{\mathrm{MI}}/\partial P)_{\Delta G}<0$, which is consistent with the behavior that T_{MI} decreases with increasing pressure. From the thermodynamic point of view, melting of the CD in $ANiO_3$ (A=Bi, Pr, Nd, …) is phenomenologically similar to a phase transition from the ice to the water near the triple point.

In summary, we found that pressure ($P\geqslant 3$ GPa) and La substitution ($x\geqslant 7.5\%$) suppressed the A-site CD of $BiNiO_3$ in essentially the same manner at room temperature, which was detected by the structural transformation from the triclinic to the orthorhombic perovskite accompanied by a steep drop of resistivity. In addition, temperature-induced melting of the CD in $Bi_{0.95}La_{0.05}NiO_3$ has clearly observed near 340 K. From the detailed structural studies combined with the transport and the magnetic measurements, we describe the charge distribution of the orthorhombic phase as $[A^{3+}\underline{L}^{\delta}, Ni^{2+}\underline{L}^{1-\delta}]$. Finally, a P-T phase diagram of $BiNiO_3$ indicating a critical point ($\sim$3 GPa and 300 K) is given, which implies a general picture of ligand-hole dynamics in $ANiO_3$. A large inhomogeneous region exists adjacent to both the metallic and the insulating regions. The present material provides an intriguing aspect of perovskite oxides in the sense that strong covalency of Bi ion at the A site causes the MI transition dominated by fluctuation of the ligand hole between the A and B sites.

ACKNOWLEDGMENTS

The authors thank M. Lee, T. Mizokawa, and H. Wadati for fruitful discussions. This work is supported by the MEXT of Japan for Grants-in-Aid for Scientific Research A14204070, Grants-in-Aid for COE Research on Elements Science, and Grants-in-Aid for 21st Century COE Programs at Kyoto Alliance for Chemistry. The synchrotron radiation experiments were performed at the SPring-8 with the approval of the Japan Synchrotron Radiation Research Institute.

*Present address: Department of Applied Physics, Waseda University, Ookubo, Shinjuku, Tokyo 169-8555, Japan. Email address: ishiwata@htsc.sci.waseda.ac.jp

[1] C. H. Chen, S-W. Cheong, and H. Y. Hwang, J. Appl. Phys. **81**, 4326 (1997).
[2] Y. Tokura and Y. Tomioka, J. Magn. Magn. Mater. **200**, 1 (1999).
[3] N. Ichikawa, S. Uchida, J. M. Tranquada, T. Niemöller, P. M. Gehring, S.-H. Lee, and J. R. Schneider, Phys. Rev. Lett. **85**, 1738 (2000).
[4] T. Yamauchi, Y. Ueda, and N. Mori, Phys. Rev. Lett. **89**, 057002 (2002).
[5] M. Takano, N. Nakanishi, Y. Takeda, S. Naka, and T. Takeda, Mater. Res. Bull. **12**, 923 (1977).
[6] P. M. Woodward, D. E. Cox, E. Moshopoulou, A. W. Sleight, and S. Morimoto, Phys. Rev. B **62**, 844 (2000).
[7] J. A. Alonso, J. L. García-Muñoz, M. T. Fernández-Díaz, M. A. G. Aranda, M. J. Martínez-Lope, and M. T. Casais, Phys. Rev. Lett. **82**, 3871 (1999).
[8] J. A. Alonso, M. J. Martínez-Lope, M. T. Casais, J. L. García-Muñoz, M. T. Fernández-Díaz, M. A. G. Aranda, Phys. Rev. B **64**, 094102 (2001).
[9] T. Saito, M. Azuma, E. Nishibori, M. Takata, M. Sakata, N. Nakayama, T. Arima, T. Kimura, and M. Takano, Physica B **329-333**, 866 (2003).
[10] M. Medarde, J. Phys.: Condens. Matter **9**, 1679 (1997).
[11] X. Obradors, L. M. Paulius, M. B. Maple, J. B. Torrance, A. I. Nazzal, J. Fontcuberta, and X. Granados, Phys. Rev. B **47**, R12353 (1993).
[12] P. C. Canfield, J. D. Thompson, S-W. Cheong, and L. W. Rupp, Phys. Rev. B **47**, R12357 (1993).
[13] J.-S. Zhou, J. B. Goodenough, B. Dabrowski, P. W. Klamut, and Z. Bukowski, Phys. Rev. Lett. **84**, 526 (2000).
[14] J. L. García-Muñoz, M. Amboage, M. Hanfland, J. A. Alonso, M. J. Martínez-Lope, and R. Mortimer, Phys. Rev. B **69**, 094106

(2004).
[15] A. E. Bocquet, A. Fujimori, T. Mizokawa, T. Saitoh, H. Namatame, S. Suga, N. Kimizuka, Y. Takeda, and M. Takano, Phys. Rev. B **45**, 1561 (1992).
[16] T. Mizokawa, A. Fujimori, H. Namatame, K. Akeyama, and N. Kosugi, Phys. Rev. B **49**, 7193 (1994).
[17] M. Abbate, G. Zampieri, J. Okamoto, A. Fujimori, S. Kawasaki, and M. Takano, Phys. Rev. B **65**, 165120 (2002).
[18] S. Ishiwata, M. Azuma, M. Takano, E. Nishibori, M. Takata, M. Sakata, and K. Kato, J. Mater. Chem. **12**, 3733 (2002).
[19] M. Yoshimura, T. Nakamura, and T. Sata, Bull. Tokyo Inst. Technol. **120**, 13 (1974).
[20] D. E. Cox and A. W. Sleight, Acta Crystallogr., Sect. B: Struct. Crystallogr. Cryst. Chem. **B35**, 1 (1979).
[21] L. F. Mattheiss and D. R. Hamann, Phys. Rev. B **28**, 4227 (1983).
[22] S. Ishiwata, Ph.D. thesis, Kyoto University, 2003.
[23] E. Nishibori, M. Takata, K. Kato, M. Sakata, Y. Kubota, S. Aoyagi, Y. Kuroiwa, M. Yamakata, and N. Ikeda, Nucl. Instrum. Methods Phys. Res. A **467-468**, 1045 (2001).
[24] F. Izumi and T. Ikeda, Mater. Sci. Forum **198**, 321 (2000).
[25] S. Ishiwata, M. Azuma, and M. Takano, Solid State Ionics **172**, 569 (2004).
[26] S. Ishiwata, M. Azuma, M. Takano, E. Nishibori, M. Takata, and M. Sakata, Physica B **329-333**, 813 (2003).
[27] J.-S. Zhou, J. B. Goodenough, B. Dabrowski, P. W. Klamut, and Z. Bukowski, Phys. Rev. B **61**, 4401 (2000).
[28] M. Azuma, H. Yoshida, T. Saito, T. Yamada, T. Takano, J. Am. Chem. Soc. **126**, 8244 (2004).
[29] J. Rodríguez-Carvajal, S. Rosenkranz, M. Medarde, P. Lacorre, M. T. Fernández-Díaz, F. Fauth, and V. Trounov, Phys. Rev. B **57**, 456 (1998).
[30] G. Burns and F. H. Dacol, Solid State Commun. **48**, 853 (1983).
[31] X. Granados, J. Fontcuberta, X. Obradors, and J. B. Torrance, Phys. Rev. B **46**, 15683 (1992).
[32] J. L. García-Muñoz, J. Rodríguez-Carvajal, P. Lacorre, and J. B. Torrance, Phys. Rev. B **46**, 4414 (1992).